

An Efficient Electrochemical Sensor Based on Ag Nanoparticle Decorated MnO₂/reduced Graphene Oxide Ternary Nanocomposite for Detection of Acetaminophen in Human Urine Sample

Murugan Keerthi¹, Gopal Boopathy¹, Shen-Ming Chen^{1,*}, Tse-Wei Chen^{1,2}, Syang-Peng Rwei^{2,3}, Xiaoheng Liu^{4,*}

¹ Department of Chemical Engineering and Biotechnology, National Taipei University of Technology, Taipei 106, Taiwan.

² Research and Development Center for Smart Textile Technology, National Taipei University of Technology, Taipei 106, Taiwan, ROC

³ Institute of Organic and Polymeric Materials, National Taipei University of Technology, Taipei 106, Taiwan, ROC

⁴ Key Laboratory of Education Ministry for Soft Chemistry and Functional Materials, Nanjing University of Science and Technology, Nanjing 210094, China.

*E-mail: smchen78@ms15.hinet.net, xhliu@mail.njust.edu.cn

Received: 7 October 2018 / Accepted: 13 November 2018 / Published: 30 November 2018

In this study, Ag/MnO₂@RGO ternary nanocomposite based electrochemical sensor was found to be the best for electrochemical detection of acetaminophen (ACTP). In which, reduced graphene oxide (RGO) sheets decorated with MnO₂ nanoclusters and silver nanoparticles (Ag NPs) by in situ growth of MnO₂ on graphene oxide (GO) sheets followed by co-reduction of Ag⁺ and GO. The Ag/MnO₂@RGO ternary nanocomposite possesses tremendous superiority in the ACTP sensing is mainly due to the large surface area and numerous electroactive sites. The structural and morphological characteristics of the as-synthesized nanomaterial were examined by XRD, FTIR, FE-SEM, HR-TEM, EDX. The electrochemical characteristics and catalytic behavior of the fabricated Ag/MnO₂@RGO ternary nanocomposite modified screen-printed carbon electrode for the determination of ACTP were demonstrated using electrochemical impedance spectroscopy, cyclic voltammetry, and differential pulse voltammetry. The results establish that the developed ACTP sensor exhibit a low detection limit of 0.0122 μM, the excellent linear response of 0.02-1810 μM with a good sensitivity of 4.144 μA μM⁻¹ cm⁻². The practicability of the sensor was investigated in the real sample of acetaminophen tablet and human urine sample.

Keywords: acetaminophen; chronic pain; Ag/MnO₂@RGO ternary nanocomposite; electrochemical detection; screen-printed carbon electrode.

1. INTRODUCTION

Acetaminophen (ACTP) is a drug commonly used as analgesics and antipyretics, which is utilized to relieve fever and pain involving chronic pain, neuralgia, backache, joint pain and used in osteoarthritis therapy (1, 2). The recommended doses of ACTP do not induce any harmful side effects, because it is completely metabolized to form inactive metabolites which would easily eliminate through urine. However, intake of ACTP content more than recommended doses produces toxic metabolite accumulation that will cause hepatotoxicity and nephrotoxicity which may lead to liver and kidney damage (3, 4). Hence, it is essential to determine the ACTP concentration in the medicinal field to avoid diseases (5-7). Various analytical techniques have been used for the determination of ACTP, which include gas chromatography (GC) (8), high performance liquid chromatography (HPLC), liquid chromatography-mass spectroscopy (LC-MS) (9), chemiluminescence (10), capillary zone electrophoresis (11) and spectrophotometry (12) etc. As above, the electrochemical sensors are more successive and extensive attention because of their wide linear range, low detection limit, stability, selectivity, sensitivity, good reproducibility and reproducibility (13).

Recently, graphene is one of the leading materials in electrochemistry due to its remarkable electronic and catalytic properties. It has been believed that the electrocatalytic ability of graphene could be further improved by incorporating metal oxide as nanocomposite (14). MnO_2 has attracted particular attention in the electrocatalytic application due to its low cost, high activity, and non-toxicity. In order to improve their specific surface areas and the electrocatalytic ability of the material, graphene and MnO_2 were used to modify the electrode surface (15). Moreover, the conductivity of RGO improved significantly by loading silver nanoparticles (Ag NPs) (16). Ag NPs have been extensively used in various applications due to their excellent chemical and physical properties such as high electrical conductivities, antibacterial properties and excellent catalytic properties (17-19). In this work, the Ag/ MnO_2 @RGO ternary nanocomposite was synthesized and modified with screen printed carbon electrode (SPCE) for the detection of ACTP. Furthermore, the modified electrode exhibits appreciable recoveries on the practical analysis of ACTP in a human urine sample and ACTP tablet.

2. EXPERIMENTAL SECTION

2.1. Materials and Instrumentations

Graphite (powder, <20 μm), Sodium nitrate (NaNO_3), Potassium permanganate (KMnO_4), Hydrochloric acid (HCl), Hydrogen peroxide (H_2O_2), Silver nitrate (AgNO_3), Acetaminophen and all the required chemicals were purchased from Sigma-Aldrich. The electrolyte of phosphate buffer (PB, 0.1 M) was prepared by mixing Na_2HPO_4 and NaH_2PO_4 . H_2SO_4 and NaOH were used for optimizing the pH of the solution. The morphological characterization was studied using Hitachi S-3000 H (FE-SEM) and (HR-TEM) H-7600, Hitachi, (Japan). The elemental percentage and composition of the materials were investigated with the help of Energy-dispersive X-ray (EDX) HORIBA EMAX X-ACT (Sensor +24 V = 16 W, resolution at 5.9 keV). Functional groups of the prepared material investigated

form FT-IR spectra using a Perkin-Elmer IR spectrometer. Crystalline structure confirmed via Powder X-ray diffraction (XRD) XPERT-PRO (PAN analytical B.V., The Netherlands) diffractometer with Cu K α radiation ($k = 1.54 \text{ \AA}$). The electron transfer ability was calculated through electrochemical impedance spectroscopy (EIS, EIM6ex Zahner, Germany). The electrochemical measurements were performed by cyclic voltammetry (CV) CHI 205C and differential pulse voltammetry (DPV) CHI 900 electrochemical workstations (CH Instruments Company, made in the U.S.A) with a three-electrode cell containing SPCE as the working electrode (working area = 0.071 cm^2), platinum wire as the counter electrode, and Ag/AgCl (saturated KCl) as the reference electrode. To prepare modified SPCE by simple drop cast method. First, the working electrode surface of SPCE was pre-cleaned by potential cycling between -1.0 V and 1.2 V , in 0.1 M phosphate buffer (pH 7.0) for 5 cycles at a scan rate of 25 mV s^{-1} . All the experiments were performed triplicate.

2.2. Synthesis of MnO_2/GO

The GO was prepared by modified Hummer's method from graphite powder. In the typical procedure, 60 mg of GO was dispersed in 100 mL of DI water by ultra-sonication for 1 h. Subsequently, a KMnO_4 solution (50 mg of KMnO_4 dissolved in 10 mL DI water) was added into the above solution. The above mixture was stirred using magnetic stirrer until the homogeneous solution formed. During the reaction, the color of the solution changed and the light red product was obtained. The product was separated by centrifugation, washed several time with DI water and ethanol and finally dried in a vacuum oven for 24 h at 45°C .

2.3. Synthesis of $\text{Ag}/\text{MnO}_2@\text{RGO}$ nanocomposite

In order to prepare $\text{Ag}/\text{MnO}_2@\text{RGO}$ nanocomposite, 50 mg of as-prepared MnO_2/GO was dispersed in 50 mL of DI water, sonicated for 1 h. A certain amount of AgNO_3 solution (1 mg/mL) was added into the above dispersion under vigorous stirring. Subsequently, NaOH solution ($0.5 \text{ M}/0.25$) was gradually introduced into the above mixture dropwise and stirred for 3h. The resulting mixture was transferred into a 100 mL round-bottomed flask and refluxed for 1 h at 90°C . Finally, the obtained product was separated by centrifugation, washed several times with DI water and ethanol to remove any unreacted molecules and dried in a vacuum oven for 24 h at 45°C . The resulting product was denoted as $\text{Ag}/\text{MnO}_2@\text{RGO}$ ternary nanocomposite.

In this nanocomposite synthesis, firstly GO act as not only a reductant but also serve as a substrate for anchoring MnO_2 nanoparticles. Secondly, $\text{Ag}/\text{MnO}@\text{RGO}$ ternary nanocomposite was formed by adding AgNO_3 and NaOH into the MnO_2/GO aqueous solution subsequently. Here, GO sheets are highly negatively charged in aqueous solution due to the presence of oxygen functional groups on the surface and edges. When adding the AgNO_3 into the MnO_2/GO dispersion, Ag ions were absorbed on the surface of GO through electrostatic interaction. When NaOH introduced into the mixture, the phenolic hydroxyl groups on GO underwent deprotonation to phenolate anions. The phenolate anions would transfer electrons to Ag ions to form metallic Ag. Meanwhile, GO was converted into RGO under alkaline

condition. Therefore, the presence of NaOH not only accelerated the reduction of Ag ions into Ag but also induce to the reduction of GO into RGO. As a result, Ag nanoparticles were in situ formed on the surface of RGO sheets, and Ag/MnO@RGO ternary nanocomposites were obtained.

3. RESULTS AND DISCUSSION

3.1. Structural characterization of Ag/MnO₂@RGO nanocomposite

The XRD patterns of GO and Ag/MnO₂@RGO nanocomposite are shown in Figure 1A. The strong peak at 10.5° corresponds to the reflection from (001) plane and well matched with the previously reported studies of GO (20). In the XRD pattern of Ag/MnO₂@RGO, the characteristic peak of GO disappeared and broad diffraction peak appears at 26°, which corresponding to the (310) plane indicates the tetragonal structure of α -MnO₂ (JCPDS-44-0141) (21). In addition, which shows four new diffraction peaks located at about 38.1°, 44.3°, 64.4°, and 77.4°, which corresponding to the (111), (200), (220), and (311) plane confirms the face-centered cubic (fcc) phase of Ag nanoparticles (JCPDS No. 65-2871) (22), exhibiting the successful reduction of Ag⁺ ions in the Ag/MnO₂@RGO composite.

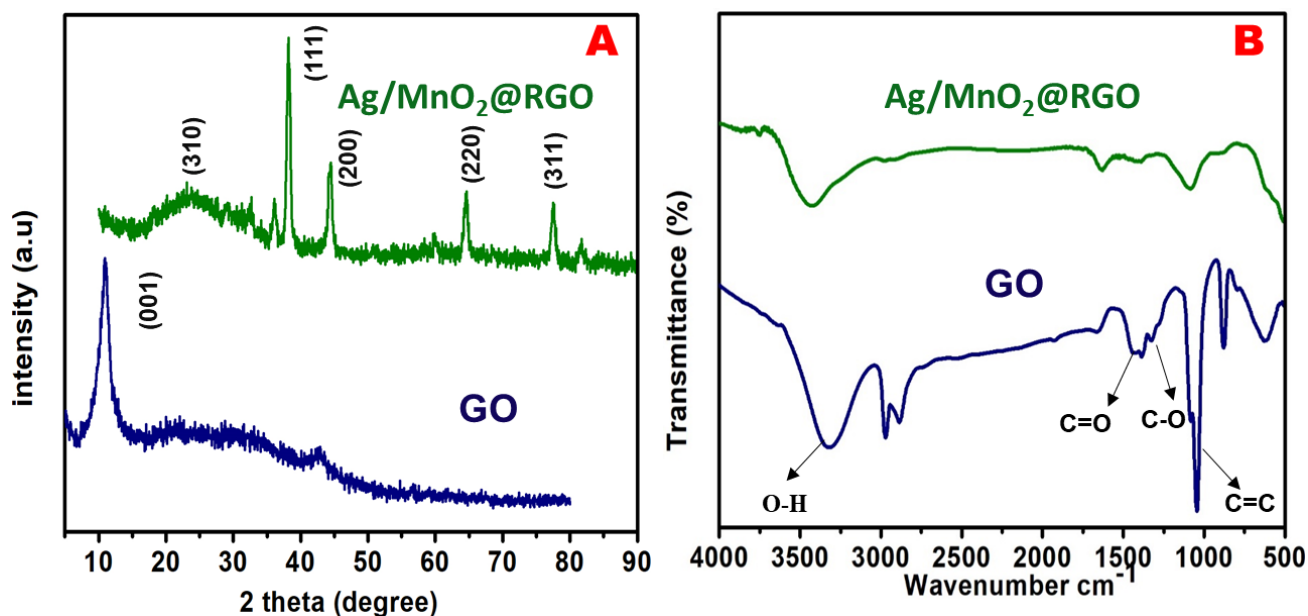


Figure 1. (A) PXRD spectrum, and (B) FT-IR spectrum of GO and Ag/MnO₂@RGO nanocomposite.

The FT-IR spectrum of the GO and Ag/MnO₂@RGO nanocomposite are displayed in (Figure. 1B). GO spectrum shows the peaks at 3415 cm⁻¹ and 1420 cm⁻¹ responsible for vibration and deformation peaks of O-H groups, respectively. The peaks at 1071 cm⁻¹ and 1630 cm⁻¹ is responsible for C-O stretching and C=C stretching, skeletal vibrations from unoxidized graphitic domains, respectively (23). In the spectrum of Ag/MnO₂@RGO, almost all the peaks from oxygen-containing functional groups were disappeared and a new band at 1570 cm⁻¹ appears due to skeletal vibration of graphene sheets (22). Which result further confirms that the GO has been well reduced in the Ag/MnO₂@RGO nanocomposite.

3.2. Morphological characterization of Ag/MnO₂@RGO nanocomposite

The morphology and structure of the as-synthesized Ag/MnO₂@RGO nanocomposite were characterized by FE-SEM and HR-TEM. Figure 2A shows an FE-SEM image of MnO₂/GO, where MnO₂ nanoparticles present as numerous ultrathin nanosheets. It can be seen that numerous clusters of mesoporous MnO₂ nanosheets covered with GO sheets by electrostatic interaction between highly negatively charged GO sheets and positively charged Mn²⁺ ions. FE-SEM image of the Ag/MnO₂@RGO reveals the surface of RGO sheets densely covered with MnO₂ sheets and Ag nanoparticles (Figure 2B). HR-TEM image of the Ag/MnO₂@RGO are shown in Figure 2C for further understanding the morphology, in which silver nanoparticles situ formed on the surface of RGO sheets, as a result, Ag/MnO₂@RGO nanocomposite was formed. The EDAX spectrum and corresponding mapping images of Ag/MnO₂@RGO nanocomposite clearly indicated that the existence of Ag, Mn, C and O with a weight percentage of 14.2, 42.7, 27.2 and 15.9 respectively (Figure 2D-I).

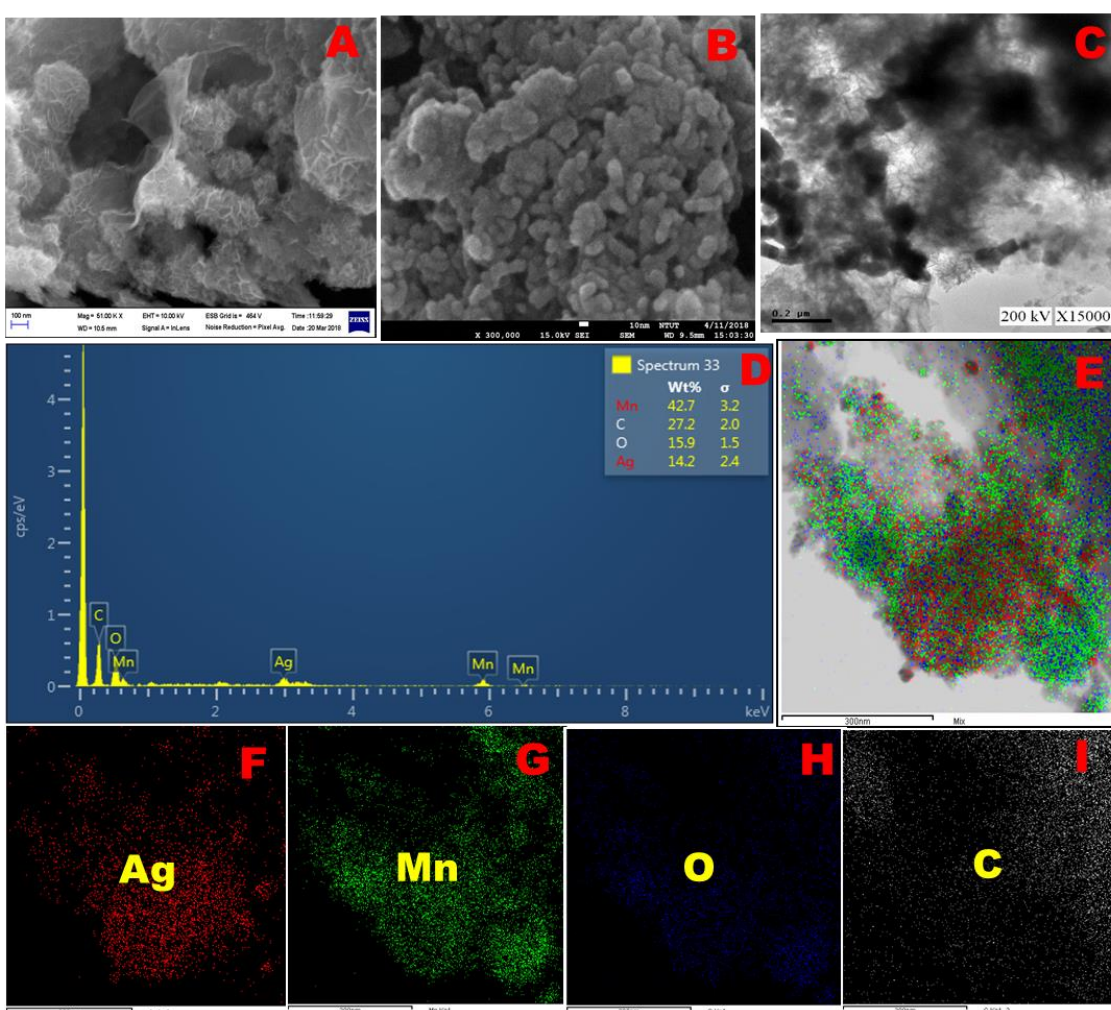


Figure 2. (A) FE-SEM image of MnO₂/GO, and (B) Ag/MnO₂@RGO. (C) TEM image of Ag/MnO₂@RGO nanocomposite. (D) EDX spectrum; Insets: Quantitative analyses and (E-I) Mapping images of Ag/MnO₂@RGO nanocomposite.

3.3. The electrocatalytic ability of Ag/MnO₂@RGO/SPCE

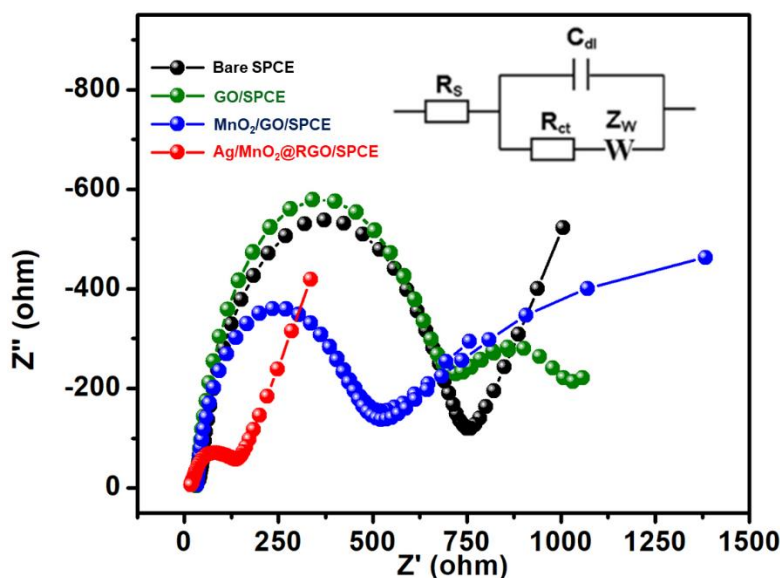


Figure 3. Electrochemical impedance spectra of bare, GO, GO/MnO₂ and Ag/MnO₂@RGO modified SPCE in 5 mM [Fe(CN)₆]^{-3/-4} with 0.1 M KCl solution, Inset; Randles circuit diagram.

The electron transfer ability of the bare SPCE and modified SPCE were studied by electrochemical impedance spectroscopy (EIS) in 5 mM [Fe(CN)₆]^{-3/-4} with 0.1 M KCl solution (Figure 3). The EIS data of bare SPCE, GO, GO/MnO₂ and Ag/MnO₂@RGO modified SPCE were plotted using the Randles circuit model (Inset: Figure 3). Where, R_{ct} , R_s , Z_w , and C_{dl} were portraying charge transmission resistance, electrolyte resistance, Warburg impedance, and double layer capacitance, respectively. From this EIS plot, it can be seen that all the modified and bare electrode exhibited semicircles of different diameters which correspond to different R_{ct} value. The R_{ct} value obtained for bare SPCE, GO, GO/MnO₂ and Ag/MnO₂@RGO modified SPCE was 715.2 Ω , 687.6 Ω , 490 Ω , and 119.2 Ω respectively. Furthermore, the Ag/MnO₂@RGO/SPCE displays the very smaller semicircle ($R_{ct} = 119 \Omega$) compared to other modified and bare electrode due to the higher electron transfer ability of Ag/MnO₂@RGO nanocomposite.

3.4. Electrochemical detection of ACTP using Ag/MnO₂@RGO/SPCE

The electrochemical behavior of ACTP at bare SPCE, GO, MnO₂/GO and Ag/MnO₂@RGO modified SPCE was investigated in 0.1 M (7.0) PB containing 200 μ M ACTP at a scan rate of 50 mV s⁻¹ (Figure 4). From this figure, the bare SPCE, GO and MnO₂/GO modified SPCE exhibit weak and inconsistent redox peak suggesting slow electron transfer in the electrode surface. On the other hand, Ag/MnO₂@RGO modified electrode shows well defined sharp oxidation and reduction peak in the potential of +0.478 and +0.096 V respectively. The observed peak current response was 3 times higher than that of bare SPCE. The enhancement of redox peak current due to the presence of more active sites in the Ag/MnO₂@RGO nanocomposite, which enhance the electron transfer process and adsorbed more ACTP molecules on its surface. The redox peak current values increased with increment in a

concentration of ACTP at Ag/MnO₂@RGO modified electrode and a linear relationship was noticed from the concentration of ACTP from 25 to 250 μM (Figure. 4B). The corresponding calibration plot is shown in the insert Figure 4B.

The electrochemical response of ACTP was investigated at Ag/MnO₂@RGO modified electrode in different scan rates (20 mV s⁻¹ to 200 mV s⁻¹) for understanding the electrochemical mechanism. Figure 4C reveals that the oxidation of ACTP increase with the increases in the scan rate from the range of 20 – 200 mVs⁻¹. The linearity was observed between the oxidation peak currents of ACTP and the square root of scan rates (Figure 4D).

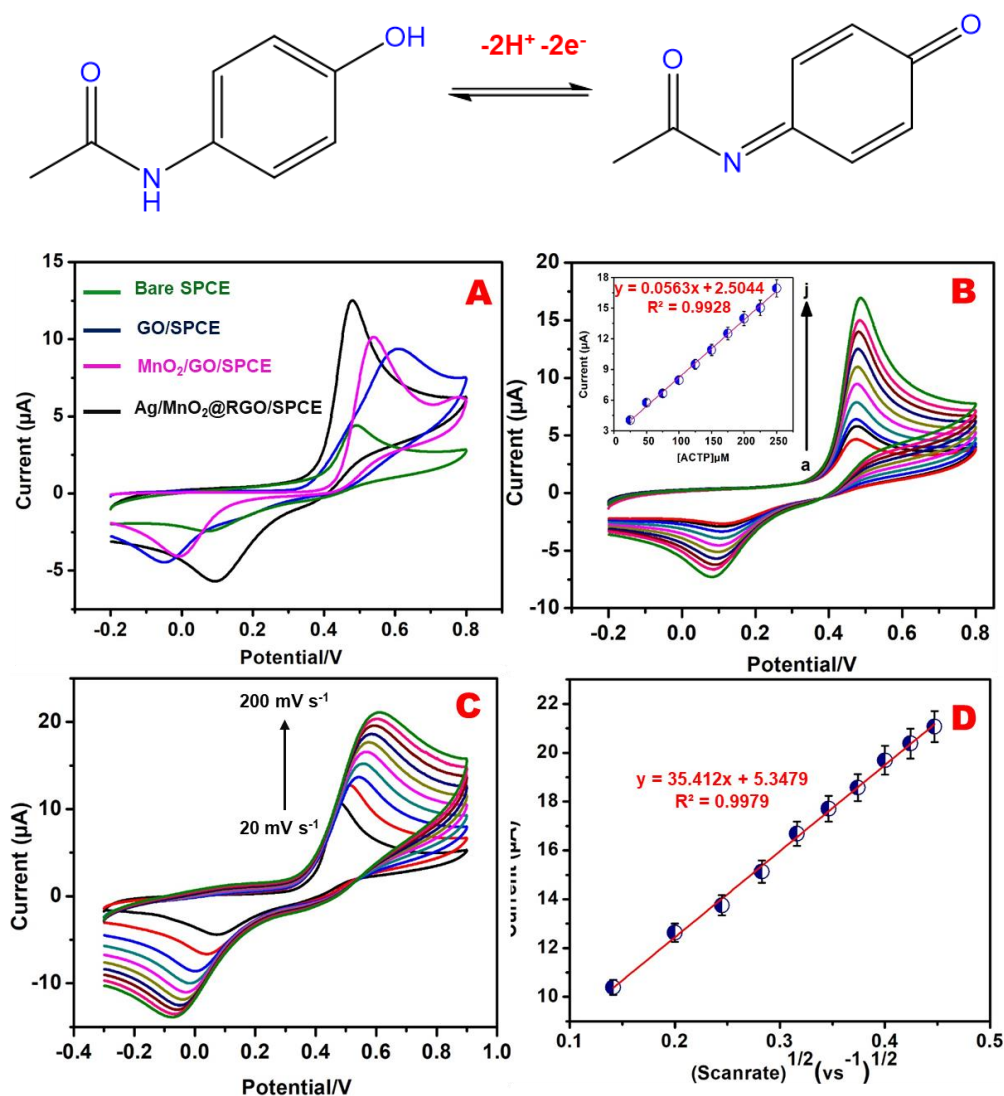


Figure 4. (A) Cyclic voltammograms of 200 μM ACTP at bare SPCE, GO, MnO₂/GO, and Ag/MnO₂@RGO modified SPCE in 0.1 M PB (pH 7); scan rate of 50 mV s⁻¹. (B) CVs of Ag/MnO₂@RGO modified SPCE in presence different concentrations of ACTP (250-250 μM) in 0.1 M PB (pH 7) at a scan rate 50 mV s⁻¹, Insert; Calibration plot of I_{pa} vs. conc. of ACTP. (C) CVs of 200 ACTP in Ag/MnO₂@RGO modified electrode at different scan rates (20 mV s⁻¹ to 200 mV s⁻¹) in 0.1 M PB (pH 7). (D) The plot of I_{pa} vs. square root of scan rate.

The linear regression equation was $I_{pa} (\mu A) = 35.412 v (Vs^{-1}) + 5.412 (R^2 = 0.997)$ and the regression suggest that ACTP at the $Ag/MnO_2@RGO$ modified electrode was a diffusion controlled process.

3.5. Effect of pH

The effect of pH range (pH 3.0–11.0) on the response of 200 μM ACTP in the PB (7.0) at $Ag/MnO_2@RGO$ modified electrode was investigated by CV (Figure 5A). The relationship of pH to the oxidation peak potential (E_{pa}) of ACTP was plotted and displayed in Figure 5C. The oxidation peak potential (E_{pa}) of the ACTP negatively shifted when increasing the pH (3.0 to 11.0), which indicates the direct involvement of the proton in the electrochemical reaction. The regression equations for ACTP were described as: $E_{pa} = -0.0432 \text{ pH} + 0.7684 (R^2 = 0.969)$. The slope value of the equation close to the theoretical value of 59 mV pH^{-1} according to the equation of the $D_{Ep}/D_{pH} = 2.303 \text{ mRT}/nF$, where m indicates a number of protons and n indicates the number of electrons involved in the reaction. Which value indicating that an electrochemical oxidation at $Ag/MnO_2@RGO$ modified electrode involved two electrons and two proton transfer process (2). Moreover, the redox peak current of ACTP increased when increasing pH 7.0 and peak current decreased further increasing the pH range (Figure 5B). Therefore, pH 7.0 was fixed as the suitable pH medium for the electrochemical detection of ACTP.

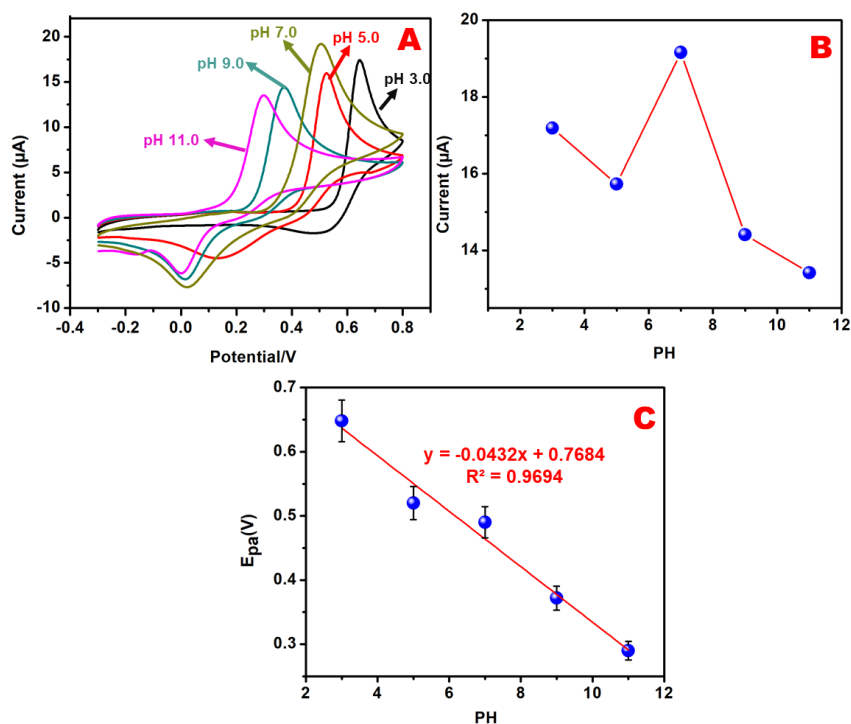


Figure 5. (A) CVs obtained for different pH (3.0, 5.0, 7.0, 9.0 and 11.0) $Ag/MnO_2@RGO$ modified SPCE containing 200 μM in 0.1 M PB (pH 7); scan rate of 50 mV/s. (B) The plot of oxidation peak current (I_{pa}) vs. pH. (C) The plot between the oxidation peak potential (E_{pa}) and pH.

3.6. DPV response of ACTP at Ag/MnO₂@RGO electrode

DPV was examined for the determination of ACTP at Ag/MnO₂@RGO modified electrode in 0.1 M PB (pH 7.0) (Figure 6A). Under the optimal experimental condition, the oxidation peaks were recorded by varying the concentration of ACTP ranging from 0.02 -1810 μM . As shown in Figure 6A, when increasing the concentrations of ACTP, the oxidation peak currents were linearly increased. At the lower concentration of ACTP, the oxidation peak current of ACTP is directly proportional to the concentration. In this case, the linearity of ACTP detection was observed to be 0.02–310 μM and the detection limit was found to be 0.012 μM . The sensitivity was calculated to be 4.144 $\mu\text{A } \mu\text{M}^{-1} \text{ cm}^{-2}$ from the slope of the lower linear response with the correlation coefficient of $R^2 = 0.995$ (Figure 6B). Furthermore, another linear range was observed in the higher concentration of ACTP concentration (410– 1810 μM), and the linearity was observed.

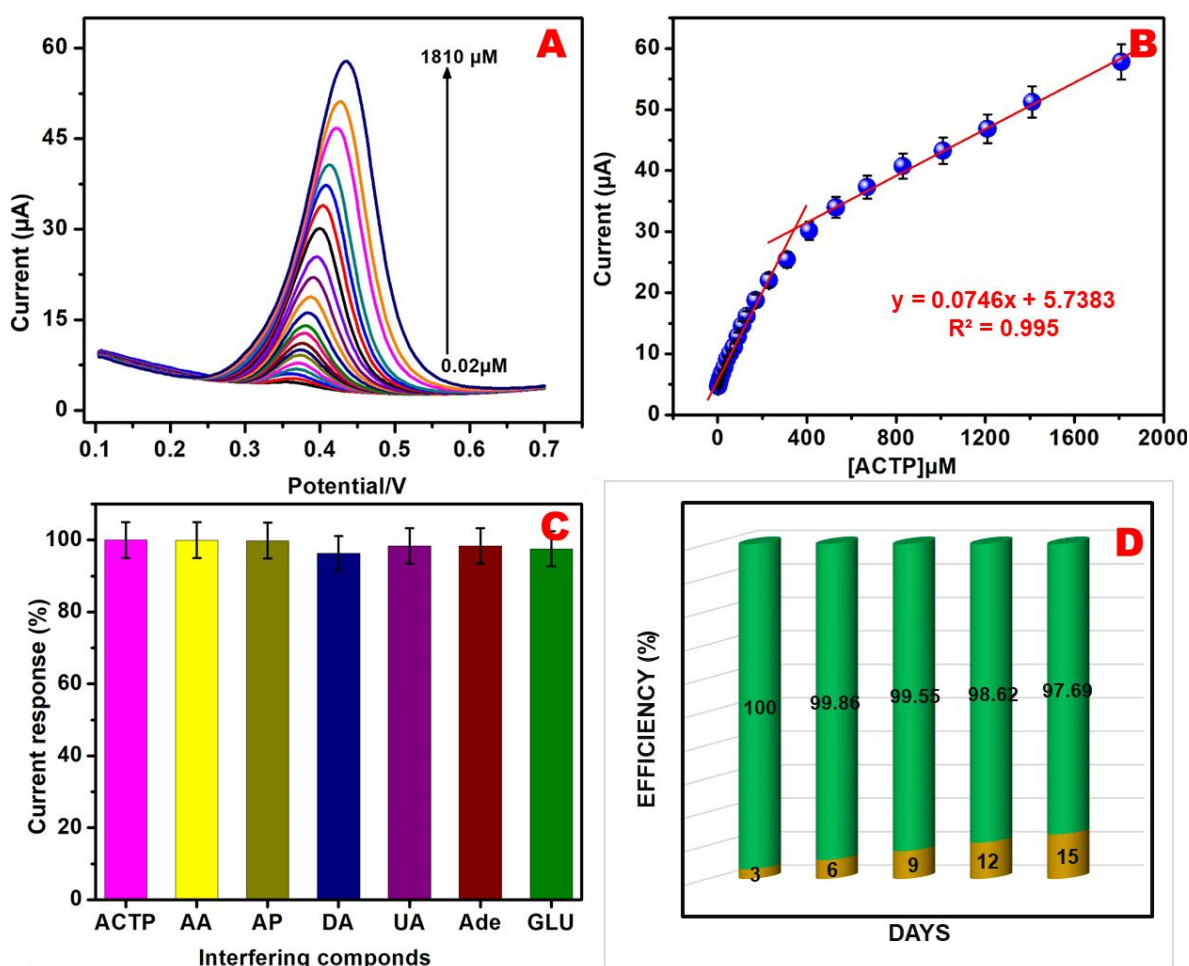


Figure 6. (A) DPV curves for the determination of ACTP at Ag/MnO₂@RGO modified electrode with continuous addition of ACTP with various concentrations (0.02 -1810 μM) in PB (pH 7.0). (B) The calibration curve of DPV current response (I_{pa}) vs. concentration of ACTP. (C) DPV responses recorded at Ag/MnO₂@RGO sensor for the addition of 50 μM ACTP with successive additions of interferents in the sequence of ascorbic acid (AA), p-aminophenol (AP), dopamine (DA), uric acid (UA), Adenine (Ade) and glucose (GLU) in PB (pH 7.0). (D) The CV responses of Ag/MnO₂@RGO modified electrode towards 50 μM ACTP in 0.1 M PB (pH 7.0), monitored for 15 days.

Moreover, the obtained analytical parameters such as a limit of detection (LOD) and linear response range can be compared with previously reported modified electrodes (Table 1). As compared with variously modified electrodes, our reported Ag/MnO₂@RGO modified SPCE offers good sensitivity, lower detection limit, and excellent linear response range for ACTP sensors.

Table 1. Comparisons of the electroanalytical parameter such as a limit of detection and linear range of proposed AgMnO₂@RGO sensor with the previously reported sensor.

Electrode	LOD (μM)	Linear range (μM)	Method	Ref.
^a f-MWCNTs/ ^b CTS-Co/ ^c GCE	0.01	0.1-400	DPV	(24)
^d g-C ₃ N ₄ nanosheets/CTS-GCE	0.15	1.70-2020	DPV	(25)
^e GO-XDA-Mn ₂ O ₃ /GCE	0.6	1-1000	CAMP	(26)
^f SPCE/ ^g CB- ^h ERGO	1.5	10-200	DPV	(27)
ⁱ AgD/ ^j RGO/GCE	0.025	0.025-500	CAMP	(28)
MWCNTs/CTS-Cu/GCE	0.024	0.1-200	DPV	(29)
^k PEDOT/Au/GCE	0.041	0.15-5881	AMP	(30)
Ag/MnO₂@RGO/SPCE	0.0122	0.02-1810	DPV	This work

^af-MWCNTs; functionalized multi walled carbon nanotubes; ^bCTS-Co; Chitosan-Cobalt; ^cGCE glassy carbon electrode, ^dg-C₃N₄; graphitic carbon nitrite; ^eGO-XDA; graphene oxide-1,4-xylenediamine; ^fSPCE; Screen printed carbon electrode; ^gCB; Carbon black; ^hERGO; electrochemically reduced graphene oxide; ⁱAgD; silver dendrites; ^jRGO; Reduced graphene oxide; ^kPEDOT; poly(3,4-ethylenedioxythiophene)

3.7. The selectivity study of Ag/MnO₂@RGO sensor

The selectivity of ACTP is a very important phenomenon for the developed electrochemical sensor because the presence of various interfering molecules affects the determination of ACTP. To study the selectivity of ACTP at Ag/MnO₂@RGO modified electrode, the potentially interfering compounds such as ascorbic acid (AA), p-aminophenol (AP), dopamine (DA), uric acid (UA), Adenine (Ade) and glucose (GLU) were used. In the experiment, Ag/MnO₂@RGO modified electrode shows well-defined oxidation peak current towards 50 μM ACTP, whereas there is no additional peak was observed for interfering molecules while the current response of ACTP not changed in the 10-fold excess addition of interfering species (Figure. 6C). This results revealed that the Ag/MnO₂@RGO modified electrode has an excellent selectivity towards ACTP in the presence of potential interferent compounds.

3.8. Stability, reproducibility, and repeatability of the Ag/MnO₂@RGO sensor

The long-term stability of Ag/MnO₂@RGO modified electrode was investigated and stored in a PB (7.0) at room temperature. After 15 days, Ag/MnO₂@RGO modified electrode has retained about 97.69 % from the initial current response (Figure. 6D). This results revealed that the Ag/MnO₂@RGO electrode has good storage stability. The reproducibility of the modified electrode was evaluated in 0.1 M PB (pH 7.0) containing 50 μM ACTP at five independent modified electrodes with the relative standard deviation (RSD) was 3.4 %, which result suggesting that acceptable reproducibility of the sensor. The repeatability of the Ag/MnO₂@RGO sensor was studied by five consecutive measurements of 50 μM ACTP with RSD of 3.2 %, indicating a good repeatability of the sensor.

3.9. Real sample analysis

The practical applicability of the Ag/MnO₂@RGO modified electrode was examined in human urine and ACTP tablet by using DPV. The real sample analysis was carried out by standard addition method. The modified electrode exhibits a well defined response in each addition of real samples. The added and obtained recovery results are given in Table 2. It was obtained that the average recoveries of ACTP were 108.35 % for Acetaminophen tablet and 99.8 % for the human urine. These results suggested that the Ag/MnO₂@RGO sensor has excellent practicability and it could be used for the determination of ACTP content in real samples.

Table 2. Determination of ACTP in Acetaminophen tablet and human urine using Ag/MnO₂@RGO modified electrode.

Real Samples	ACTP			
	Added/μM	Found/μM	Recovery/%	*RSD/%
Acetaminophen tablet	0	-	-	-
	5	5.39	107.8	3.71
	10	10.89	108.9	3.82
Human urine	0	-	-	-
	5	4.97	99.4	3.94
	10	10.02	100.2	3.20

4. CONCLUSIONS

In this work, Ag/MnO₂@RGO ternary nanocomposite electrochemical sensor was successfully constructed for the sensitive detection of ACTP. The designed ACTP sensor architecture with combining the advantages of RGO, MnO₂ and Ag NPs offer the good electrochemical catalytic properties, excellent conductivity and efficient electron transfer with fast response, wide linear range, low detection limit

(0.0122 μM , S/N=3) and excellent selectivity. Furthermore, the developed sensor also exhibits good reproducibility and stability. Finally, the practicality of our proposed sensor was verified by the determination of ACTP in acetaminophen tablet and human urine with good accuracy and high precision. All these features demonstrate that the Ag/MnO₂@RGO ternary nanocomposite shows a vast potential for the applications in electrochemical sensing platform.

ACKNOWLEDGMENT

The project was supported by the Ministry of Science and Technology (MOST 107-2113-M-027-005-MY3), Taiwan. This work also jointly supported by the projects from NTUT-NUST-107-1 and NSFC51572126, National Taipei University of Technology and Nanjing University of Science and Technology.

References

1. B.-R. Adhikari, M. Govindhan and A. Chen, *Electrochim. Acta*, 162 (2015) 198.
2. S. Yu, H. Li, G. Li, L. Niu, W. Liu and X. Di, *Talanta*, 184 (2018) 244.
3. S. Tanuja, B. K. Swamy and K. V. Pai, *J. Electroanal. Chem.*, 798 (2017) 17.
4. A. Cernat, M. Tertiş, R. Săndulescu, F. Bedioui, A. Cristea and C. Cristea, *Anal. chim. acta*, 886 (2015) 16.
5. H. Wang, S. Zhang, S. Li and J. Qu, *Talanta*, 178 (2018) 188.
6. R. N. Gomes, C. P. Sousa, P. N. Casciano, F. W. P. Ribeiro, S. Morais, P. de Lima-Neto and A. N. Correia, *Mater. Sci. Eng., C*, 88 (2018) 148.
7. H. Karimi-Maleh, M. R. Ganjali, P. Norouzi and A. Bananezhad, *Mater. Sci. Eng., C*, 73 (2017) 472.
8. N. S. Anuar, W. J. Basirun, M. Ladan, M. Shalauddin and M. S. Mehmood, *Sens. Actuators, B*, 266 (2018) 375.
9. A. Kutluay and M. Aslanoglu, *Anal. chim. acta*, 839 (2014) 59.
10. S. Biswas, D. Chakraborty, R. Das, R. Bandyopadhyay and P. Pramanik, *Anal. chim. acta*, 890 (2015) 98.
11. X.-Y. Wu, W.-J. Niu, S. Cosnier, S.-Y. Deng, X.-J. Zhang and D. Shan, *Electrochim. Acta*, 186 (2015) 16.
12. H. Ghadimi, R. M. Tehrani, A. S. M. Ali, N. Mohamed and S. Ab Ghani, *Anal. chim. acta*, 765 (2013) 70.
13. J. Li, J. Liu, G. Tan, J. Jiang, S. Peng, M. Deng, D. Qian, Y. Feng and Y. Liu, *Biosens. Bioelectron.*, 54 (2014) 468.
14. M. Keerthi, M. Akilarasan, S.-M. Chen, S. Kogularasu, M. Govindasamy, V. Mani, M. A. Ali, F. M. Al-Hemaid and M. Elshikh, *J. Electrochem. Soc.*, 165 (2018) B27.
15. S. Lu, D. Yan, L. Chen, G. Zhu, H. Xu and A. Yu, *Mater. Letters*, 168 (2016) 40.
16. J. Kim, H. Ju, A. I. Inamdar, Y. Jo, J. Han, H. Kim and H. Im, *Energy*, 70 (2014) 473.
17. I. Kodintsev, V. Tolstoy and A. Lobinsky, *Mater. Letters*, 196 (2017) 54.
18. N. Koriche, A. Bouguelia, M. Mohammedi and M. Trari, *J. Mater. Sci.*, 42 (2007) 4778.
19. L. Chen, H. Sun, Y. Zhao, Y. Zhang, Y. Wang, Y. Liu, X. Zhang, Y. Jiang, Z. Hua and J. Yang, *RSC Adv.*, 7 (2017) 16553.
20. S. Chen, J. Zhu, X. Wu, Q. Han and X. Wang, *ACS nano*, 4 (2010) 2822.
21. P.-Y. Kuang, M.-H. Liang, W.-Y. Kong, Z.-Q. Liu, Y.-P. Guo, H.-J. Wang, N. Li, Y.-Z. Su and S. Chen, *New J. Chem.*, 39 (2015) 2497.

22. L. Ma, X. Shen, Z. Ji, G. Zhu and H. Zhou, *J. Chem. Eng.*, 252 (2014) 95.
23. Z. Hu, Y. Zhao, J. Liu, J. Wang, B. Zhang and X. Xiang, *J. colloid interface sci.*, 483 (2016) 26.
24. S. Akhter, W. J. Basirun, Y. Alias, M. R. Johan, S. Bagheri, M. Shalauddin, M. Ladan and N. S. Anuar, *Anal. Biochem.*, 551 (2018) 29.
25. L. Liu, H. Lv, C. Wang, Z. Ao and G. Wang, *Electrochim. Acta*, 206 (2016) 259.
26. A. Ejaz and S. Jeon, *Electrochim. Acta*, 245 (2017) 742.
27. G. Ibáñez-Redín, D. Wilson, D. Gonçalves and O. Oliveira Jr, *J. colloid interface sci.*, 515 (2018) 101.
28. S. Dhanush, M. Sreejesh, K. Bindu, P. Chowdhury and H. Nagaraja, *Mater. Research Bulletin*, 100 (2018) 295.
29. A. Mao, H. Li, D. Jin, L. Yu and X. Hu, *Talanta*, 144 (2015) 252.
30. M. Li, W. Wang, Z. Chen, Z. Song and X. Luo, *Sens. Actuators, B* 260 (2018) 778.

© 2019 The Authors. Published by ESG (www.electrochemsci.org). This article is an open access article distributed under the terms and conditions of the Creative Commons Attribution license (<http://creativecommons.org/licenses/by/4.0/>).